TÜBİTAK

Turkish Journal of Earth Sciences

http://journals.tubitak.gov.tr/earth/

Research Article

Turkish J Earth Sci
(2016) 25: 274-287

doi:10.3906/yer-1508-9

Comparative study on geochemical characterization of the Carboniferous aluminous argillites from the Huainan Coal Basin, China

Bingyu CHEN[1,2], Guijian LIU[1,2,*], Dun WU[1], Ruoyu SUN[1]

[1]CAS Key Laboratory of Crust-Mantle Materials and the Environments, School of Earth and Space Sciences, University of Science and Technology of China, Hefei, P.R. China

[2]State Key Laboratory of Loess and Quaternary Geology, Institute of Earth Environment, Chinese Academy of Sciences, Xi'an, Shaanxi, P.R. China

Received: 28.08.2015 • **Accepted/Published Online:** 07.02.2016 • **Final Version:** 05.04.2016

Abstract: Aluminous argillites were widely deposited in the Taiyuan Formation at the Huainan Coalfield at the southeast margin of the North China Plate. However, knowledge about their formation conditions and geochemical characterizations is not presently known. We recovered underground aluminous argillites at depths of 485–610 m from a borehole in the Zhangji Coal Mine and characterized their geochemical parameters, including major and trace elements, by X-ray fluorescence, inductively coupled plasma optical emission spectrometry, and inductively coupled plasma mass spectrometry. The provenance, climatic conditions during the weathering process of parent rocks, weathering extent, and depositional environments of Huainan aluminous argillites were investigated. Results show that Huainan aluminous argillites are depleted in alkalis and alkaline earth elements and enriched in Al, Fe, and Ti. The ratios of immobile trace elements such as Nb/Ta and Zr/Hf are similar in all the argillite samples. The NASC-normalized rare earth element (REE) patterns of the argillites show an enrichment of heavy REEs and depletion of light REEs, with positive Ce and negative Eu anomalies. The provenance analysis indicates that the studied aluminous argillites probably derived from the common parent rocks composed of felsic to intermediate igneous rocks. These argillites were presumably deposited under anoxic environments.

Key words: Aluminous argillite, chemical weathering, sedimentary environment, Taiyuan Formation, Huainan

1. Introduction

The Huainan Coalfield is one of the most important coal basins in China and has been mined for a long history. Its coal-bearing sequences, from old to young, are mainly composed of the Late Carboniferous Taiyuan Formation, the Early Permian Shanxi and Lower Shihezi Formations, and the Late Permian Upper Shihezi Formation. The coal seams of the Taiyuan Formation, however, were only partially developed, and their economic values are not so competitive. Nevertheless, the coexistence of coal and shale provides a large possibility in the preservation of coal bed gases in the Taiyuan Formation. Therefore, understanding the depositional paleoenvironment of the Taiyuan Formation is critical important for resource exploration. The aluminous argillite layers are commonly used as marker beds for stratigraphic correlation in complicated depositional settings. Consequently, the geochemical characterization of aluminous argillites could be potentially used to constrain coeval depositional environments.

Geochemical parameters have been applied successfully to trace the depositional environments and paleoredox conditions of ancient sedimentary rocks such as shales, argillites, and sandstones (Clavert and Pedersen, 1993; Jones and Manning, 1994; Nath et al., 1997; Dobrzinski et al., 2004; Ghabrial et al., 2012; Dhannoun and Al-Dlemi, 2013; Meinhold et al., 2013). Chemical compositions of sedimentary rocks are influenced by various factors including source materials and their weathering degrees, transportation dynamics of clastic materials, depositional environments, and postdepositional processes (Taylor and McLennan, 1985; Hayashi et al., 1997; El-Bialy, 2013). Thus, geochemical parameters of the sedimentary rocks can be used, in turn, to trace the source materials, the degrees to which the source materials were weathered, and the contemporary depositional conditions. For example, Harnois (1988) and McLennan et al. (1993) showed that the Al_2O_3/TiO_2 values of sandstones and argillites are basically conserved from their parent rocks and could be applied in identifying the source materials. Several specific

* Correspondence: lgj@ustc.edu.cn

trace elements and rare earth elements (REEs) have been used to establish discrimination diagrams for provenance analyses (Floyd and Leveridge, 1987; Floyd et al., 1991; Zimmermann and Bahlburg, 2003; Armstrong-Altrin et al., 2004).

The present study investigates the geochemical characterizations of Upper Carboniferous aluminous argillites from the Taiyuan Formation, Huainan Coalfield, with an aim of tracing their source materials, weathering degrees of source rocks, and coeval depositional environments.

2. Geologic setting

The Huainan Coalfield is located in the southeastern North China Plate (Figure 1). The stratigraphic succession of this area includes, from oldest to youngest, the Cambrian, Lower-Middle Ordovician, Upper Carboniferous, Permian, Lower and Upper Triassic, Jurassic, Cretaceous, Tertiary, and Quaternary. Due to the Middle Caledonian movement, the Huainan basin began to lift at the end of the Early-Middle Ordovician and then underwent a long-term denudation until the Late Carboniferous. This caused an absence of strata of the Upper Ordovician, Silurian, Devonian, and Lower and Middle Carboniferous. At the early stage of the Late Carboniferous, Huang-Huai seawater invaded the neighboring Huaibei area, and a transitional face named the Benxi Formation was deposited (Figure 2). Because the southern uplift of the Bengbu strata slowed down the southern seawater transgression, no sediments were preserved in the Huainan area until the late stage of the Late Carboniferous, when a transitional sedimentary facies named the Taiyuan Formation was formed. Following the Taiyuan Formation, the Shanxi Formation and Lower Shihezi Formation of the Lower Permian and the Upper Shihezi Formation and Shiqianfeng Formation of the Upper Permian were continuously deposited (Sun et al., 2010; Chen et al., 2011; Yang et al., 2011).

Limestone, sandstone, silty claystone, and aluminous argillite are the main lithological constituents of the Taiyuan Formation, accompanied by unworkable coal seams and carbonaceous claystone. The thickness of the Carboniferous Taiyuan Formation in the Huainan Coalfield is 100–130 m, comprising 11–13 layers of limestone (Figure 3). The Taiyuan Formation stratum in the present study is 129 m in thickness and comprises 48 m of limestone and 19 m of aluminous argillite.

3. Sampling and analysis

Two bauxitic argillites (Z-1 and Z-2), 8 aluminous argillites (Z-3, Z-4, Z-5, Z-6, Z-7, Z-8, Z-9, and Z-10), and 3 limestone samples (Z-11, Z-12, and Z-13) were collected from the ZJBY1 borehole (32°46′38″N, 116°29′45″E) during the exploration stage of the Zhangji Coal Mine at the Huainan Coalfield. Aluminous argillites were collected from 3 layers of aluminous argillite, A1, A2, and A3, overlying limestone layers of L4, L7, and L11, respectively (Figure 3). The upper 0.3 m of A1 is a thin layer of bauxite where 2 bauxitic argillites were collected. Z-3, Z-4, Z-5, and Z-6 were collected from the lower part of A1; Z-7 and Z-8 were collected from A2; and Z-9 and Z-10 were collected from A3. Z-11, Z-12, and Z-13 were collected from the limestone layers of L4, L7, and L11, respectively (Figure 3).

Bulk samples were manually grinded in a quartz mortar and then sieved through a 230 mesh screen to obtain homogenized samples. An aliquot of ~0.2 g of powdered sample was accurately weighed and then was fully digested with mixed acids (HNO_3 : HCl : HF = 3:1:1) in a microwave digestion instrument (Multiwave 3000, Anton Paar GmbH).

Major oxides of the samples were determined by XRF. Loss on ignition (LOI) of the samples was determined gravimetrically by calculating the mass difference between 1000 °C calcined sample residual and the original 2 g of sample. Selected trace elements (B, Mn, Ni, and Zn) were determined by inductively coupled plasma optical emission spectrometry (ICP-OES; Optima 7300 DV, PerkinElmer), while other trace elements (V, Cr, Co, Sr, Ba, Pb, Zr, Nb, Hf, Ta, and Th) and REEs were determined by inductively coupled plasma mass spectrometry (ICP-MS; X Series 2, Thermo Fisher Scientific). The uncertainties for most of the elements determined, as evaluated by various certified reference materials, were within 5%.

4. Results

4.1. Major oxides

In the 3 layers of aluminous argillite samples, SiO_2 and Al_2O_3 are the dominant constituents, with their contents ranging from 33.1% to 64.9% and from 24.3% to 30.5%, respectively (Table 1). Iron oxides (expressed as TFe_2O_3) and TiO_2 are the secondary components in aluminous argillite, varying from 1.5% to 17.6% and 0.9% to 1.6%, respectively. Alkalis and alkali earth oxides (Na_2O: 0.3%–1.2%; K_2O: 0%–2.8%; MgO: 0%–0.7%; CaO: 0.1%–0.7%) are present at low concentrations in aluminous argillite. Similar to the aluminous argillites, bauxitic argillites are also enriched in Al_2O_3 and SiO_2, and depleted in alkalis and alkalis earth oxides. The high Al contents in bauxitic argillites (28.5% and 36.9%) are probably caused by intense chemical weathering. In the underlying limestone samples (Z-11, Z-12, and Z-13), CaO is the predominate component with its concentrations varying from 43.1% to 48.2%. The concentrations of Al_2O_3, Fe_2O_3, and SiO_2 are 0.1%–1.8%, 0.4%–1.4%, and 1.2%–4.8%, respectively.

Significant correlations can be seen between selected major oxides of the argillites (Table 2; Figure 4). SiO_2

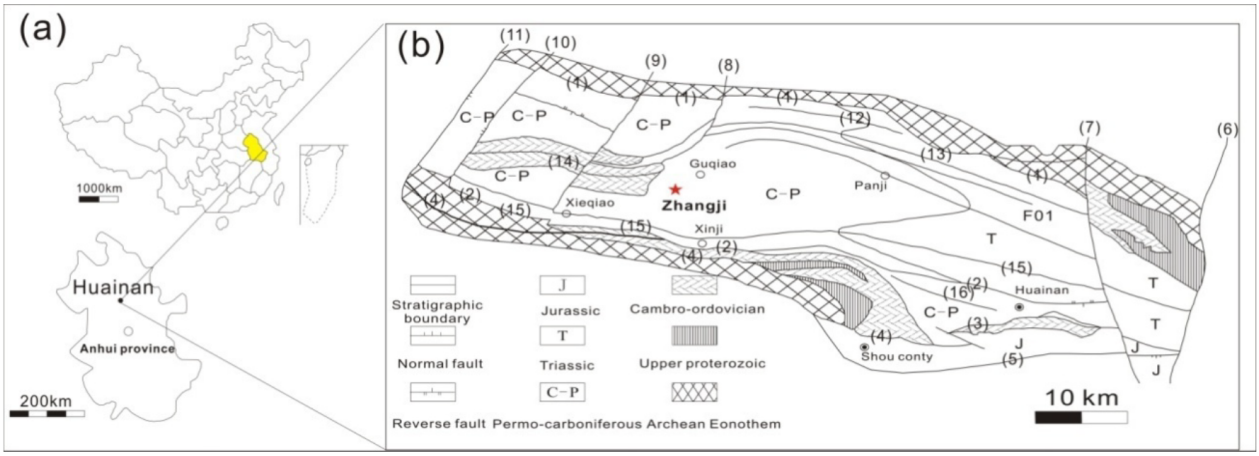

Figure 1. a) Location of Anhui Province and the Huainan Coalfield. b) Tectonic geological map of the Huainan Coalfield and location of the Zhangji Coal Mine. 1): Shangyao-Minglongshan thrust fault; 2): Fufeng thrust fault; 3): Shungengshan thrust fault; 4): Fuli thrust fault; 5): Shouxian-Laorencang normal fault; 6): Wudian fault; 7): Guzhen-Changfeng fault; 8): Guqiao fault; 9) Chenqiao fault; 10): Jiangkouji fault; 11): Wanghutong fault; 12): Zhuji-Tangji anticline; 13): Shangtang-Gengcun syncline; 14): Chenqiao-Panji anticline; 15): Xieqiao-Gugou syncline; 16): Lutang anticline.

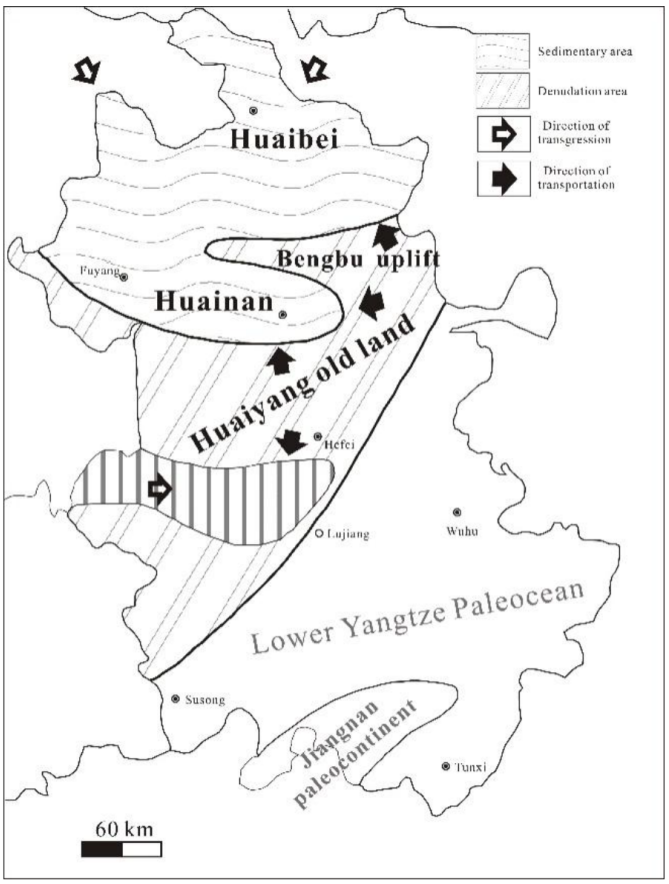

Figure 2. Lithofacies and paleogeography of the Huainan Coalfield during the Late Carboniferous period (modified from the Regional Geology Department of Anhui Province).

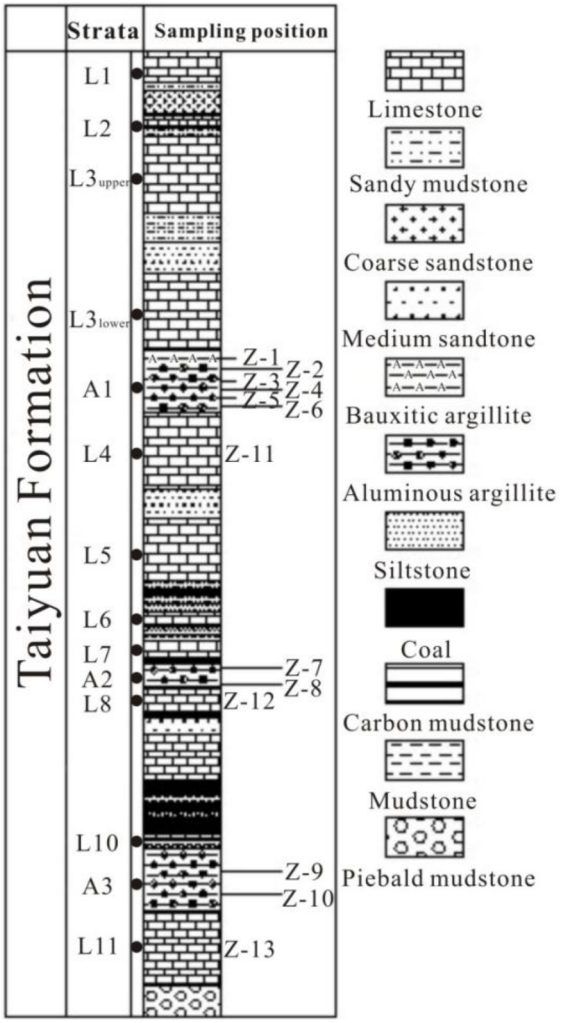

Figure 3. Sedimentary sequence of the Late Carboniferous Epoch Taiyuan Formation in the Zhangji Coalmine.

positively correlates with Na_2O, MgO, K_2O, and CaO, but negatively correlates with Al_2O_3, TiO_2, and Fe_2O_3. Elements such as Al, Ti, and Fe are immobile and not susceptible to chemical weathering processes. Their oxides show negative correlations with SiO_2. In contrast, the oxides of mobile elements such as Na, K, Mg, and Ca show positive correlations with SiO_2. Nearly all the argillites have comparable ratios of SiO_2/Al_2O_3, Fe_2O_3/Al_2O_3, and TiO_2/Al_2O_3 (Figure 4), suggesting that they were possibly derived from the same source materials. However, one bauxitic argillite, Z-1, significantly deviates from the correlation slopes of SiO_2 vs. Al_2O_3 and Fe_2O_3 vs. Al_2O_3 in Figure 4, which indicates that it probably suffered a more extensive lateritization than other argillite samples.

4.2. Trace elements

During chemical weathering, variable amounts of mobile trace elements, such as Sr, Ba, and Eu can be depleted, while ratios between different immobile elements could remain stable from parent rocks to final sedimentary rocks (Floyd and Leveridge, 1987; Floyd et al., 1991; Zimmermann and Bahlburg, 2003; Armstrong-Altrin et al., 2004).

Strontium and Ba are commonly sensitive to the change of sedimentary aqueous environments (Francois, 1988; Torres et al., 1996; Schmitz et al., 1997). Strontium (4.85–166.15 μg/g) and Ba (2.76–263.25 μg/g) vary significantly in the aluminous argillites, but are significantly lower than those in the limestone samples (3728–4985 μg/g for Sr and 58–114 μg/g for Ba; Table 3).

Nb, Ta, Zr, and Hf are often enriched along with the processes of chemical weathering and do not have significant variations during subsequent transport and deposition processes. There are significant differences in Nb, Ta, Zr, and Hf between limestone and aluminous argillite samples.

Figure 5 shows the distribution of NASC-normalized REEs in the studied aluminous argillite samples. The REEs of all the aluminous argillites have La_N/Yb_N values of less than 0.4, indicating a significant enrichment of heavy REEs (HREEs) relative to light REEs (LREEs). In addition, nearly all the aluminous argillite samples display positive Ce anomalies ($Ce/Ce^* = 1.39$, ranging from 1.15 to 1.91, except one sample, Z-8, of 0.89) and negative Eu anomalies ($Eu/Eu^* = 0.19$, ranging from 0.17 to 0.23). The REE parameters of aluminous argillites are very different from the underlying limestone samples, which show negative Ce anomalies and positive Eu anomalies.

5. Discussion

5.1. Source rocks

5.1.1. Evidence from stratigraphic succession

There are two potential source rocks for the studied high-Al argillites: near-field underlying limestone and far-field silicate rocks. According to previous studies (Liu, 1987; Lan et al., 1988; Sun et al., 2010; Chen et al., 2011), transgression and regression of seawater occurred frequently in the Huainan Coal Basin during the late stage of the Late Carboniferous. If these argillites were developed as the leaching and weathering products of the underlying limestone in a similar manner as karst bauxites, calcite and dolomite should contribute substantial proportions to the mineral composition of the studied argillites. However, the contents of CaO and MgO in aluminous argillite are <1%, which is significantly lower than in underlying limestone samples (43%–48% for CaO and 3.1%–3.5% for MgO) (Table 1). Hence, the potential source material for the studied argillites is thought to be the silicate rocks.

5.1.2. Evidence from major oxides

Al_2O_3 and TiO_2 in source rocks are usually preserved in the clastic sedimentary rocks, because Al and Ti are not

Table 1. Major oxide concentrations (wt. %) for the bauxitic argillites (BA, Z-1, and Z-2) and aluminous argillites (AA, Z-3, to Z-10), and the underlying limestone samples (LS, Z-11, to Z-13) of the Taiyuan Formation, Huainan Coalfield.

Sample	Lithology	Al_2O_3	SiO_2	Fe_2O_3	TiO_2	CaO	K_2O	P_2O_5	Na_2O	MgO	MnO	LOI	CIA
Z-1	BA	36.92	42.39	4.44	2.116	0.08	0.10	0.037	0.13	0.15	0.101	11.56	98.75
Z-2	BA	28.52	41.19	12.75	1.326	0.16	0.17	0.055	0.15	0.32	0.045	12.34	97.53
Z-3	AA	26.64	44.22	9.93	1.16	0.16	1.27	0.069	0.32	0.06	0.046	9.25	92.40
Z-4	AA	27.94	45.98	10.41	1.26	0.24	1.34	0.07	0.60	0.18	0.047	9.93	90.67
Z-5	AA	29.93	33.12	17.64	1.55	0.09	0.03	0.049	0.64	0.01	0.005	13.96	95.99
Z-6	AA	30.47	33.37	17.04	1.56	0.07	0.03	0.046	0.52	0.01	0.005	17.90	96.78
Z-7	AA	24.32	62.65	1.51	0.94	0.69	2.73	0.072	1.22	0.60	0.003	3.26	79.64
Z-8	AA	26.28	64.92	1.49	0.99	0.72	2.76	0.067	1.20	0.67	0.003	2.30	80.74
Z-9	AA	29.73	45.17	8.20	1.09	0.19	1.78	0.076	0.65	0.18	0.005	7.93	89.90
Z-10	AA	29.36	44.53	8.25	1.09	0.18	1.78	0.08	0.58	0.18	0.011	14.96	90.15
Z-11	LS	0.11	3.1	0.37	0.01	46.46	0.04	0.071	0.51	3.46	0.031	42.84	0.13
Z-12	LS	0.16	1.24	0.40	0.01	48.18	0.02	0.118	0.52	3.26	0.044	45.05	0.18
Z-13	LS	1.79	4.84	1.44	0.04	43.07	0.45	0.21	0.63	3.12	0.041	42.38	2.19

Table 2. Pearson's correlation coefficients between major oxides in the studied aluminous argillites.

	SiO_2	Al_2O_3	Na_2O	MgO	K_2O	TiO_2	MnO	CaO	Fe_2O_3
SiO_2	1								
Al_2O_3	–0.85	1							
Na_2O	0.83	–0.63	1						
MgO	0.97	–0.77	0.94	1					
K_2O	0.95	–0.75	0.71	0.89	1				
TiO_2	–0.88	0.72	–0.56	–0.77	–0.97	1			
MnO	–0.13	–0.16	–0.55	–0.33	–0.11	0	1		
CaO	0.96	–0.83	0.93	0.99	0.86	–0.74	–0.28	1	
Fe_2O_3	–0.97	0.8	–0.74	–0.91	–0.99	0.96	0.12	–0.89	1

readily mobilized by weathering processes (Harnois, 1988; McLennan et al., 1993; El-Bialy, 2013; Abedini and Calagari, 2014). Hayashi et al. (1997) demonstrated that the Al_2O_3/TiO_2 ratios of sandstones and mudstones changed insignificantly during the weathering of source rocks and the subsequent transportation, deposition, and diagenesis of sediments. A discriminating criterion has been applied to distinguish different types of parent igneous rocks, with Al_2O_3/TiO_2 ratios of 3–8 for mafic igneous rocks (SiO_2 = 45.52%), 8–21 for intermediate igneous rocks (SiO_2 = 53%–66%), and 21–70 for felsic igneous rocks (SiO_2 = 66%–76%). The Al_2O_3/TiO_2 ratios of the studied argillites samples range from 19.31 to 27.28 (mean = 23.83; Figure 6), suggesting that they were possibly derived from felsic to intermediate igneous rocks (Amajor, 1987; Imchen et al., 2014).

The A-CN-K triangular diagram proposed by Nesbitt and Young (1984) is also commonly used to empirically indicate the types of original rocks (Fedo et al., 1995; Babechuk et al., 2014). According to the difference between the removal rates of Na and Ca from plagioclase and of K from microcline, the initial weathering trends of igneous rocks are subparallel to the $(CaO+Na_2O)$-Al_2O_3 sideline. This trend could change when the difference in their removal rates is nonsignificant. The weathering trend of our studied argillites is approximately perpendicular to the $(CaO+Na_2O)$-K_2O boundary, and it points to the Al_2O_3 apex (Figure 7). As pointed out by Fedo et al. (1995) and El-Bialy (2013), the source materials can be reliably inferred if the studied weathering trend is extrapolated backwards to the plagioclase and K-feldspar connecting line. Using this extrapolation method, the potential source

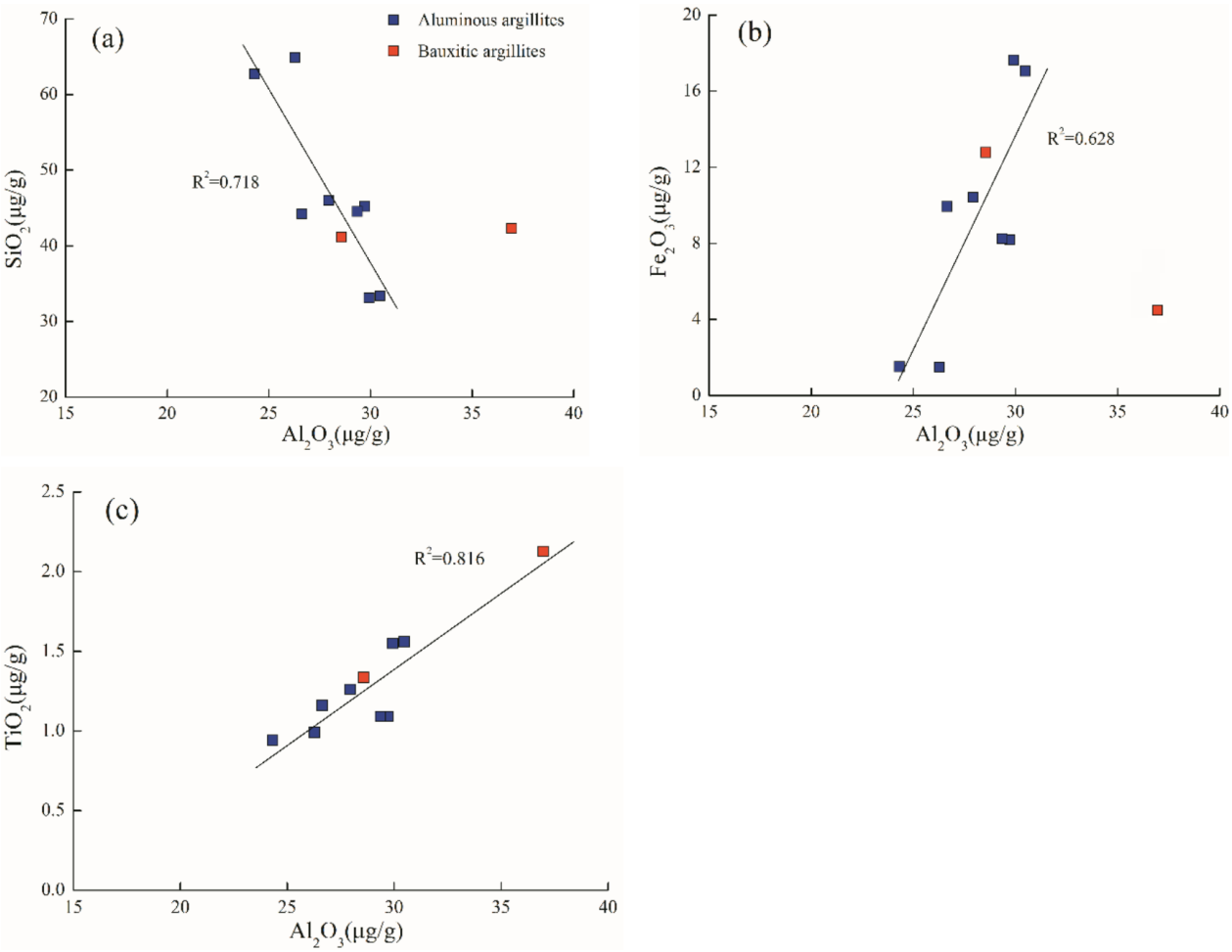

Figure 4. Plots of Al_2O_3 vs. SiO_2 (A), vs. Fe_2O_3 (B), and vs. TiO_2 (C) in the studied bauxitic and aluminous argillites.

materials in the studied argillites could be felsic igneous rocks (granodiorite and granite) (Figure 7).

5.1.3. Evidence from trace elements

The ratios between these specific elements (e.g., Zr, Hf, Nb, Ta) in sedimentary rocks can be used for the provenance analysis. Figure 8 compares the TiO_2 vs. Zr of the studied aluminous argillite with previously defined source rock fields (Jolly, 1980; Stone et al., 1987; Paradis et al., 1988; Lafleche et al., 1992; Hayashi et al., 1997). In the TiO_2 vs. Zr diagram, aluminous argillites fall in the intermediate igneous rock field, near the boundary of acidic and intermediate igneous rocks. Our studied aluminous argillite samples have a mean Zr/Hf ratio of 33.19 (from 27.64 to 33.77), which is slightly lower than the granite Zr/Hf value of 33.5–39.8 (Panahi et al., 2000) but higher than the basic-ultrabasic rock Zr/Hf value of 18.38 (from 11.38 to 24.85) (Calagari and Abedini, 2007). This indicates again that our aluminous argillites are predominately sourced from intermediate igneous rocks.

Nevertheless, it does not exclude the possibility of acidic source rocks. From the TiO_2-Ni discrimination diagram of Floyd et al. (1989) (Figure 9), two of the argillites lie in the acidic rock field, although most of the argillites are in the intermediate igneous rock field. Our argillites show an enrichment of HREEs relative to LREEs, with positive Ce anomalies and significant negative Eu anomalies. This indicates that the source rocks are not acidic-intermediate igneous rocks, in contradiction to the inferences from the above elements. We speculate that the REEs in source rocks are possibly significantly fractionated by weathering processes and postdepositional processes of the argillites. However, the significant Eu anomaly is likely imparted by source rocks and is less modified by the weathering of source rocks to the final deposition of argillites.

5.2. Climate conditions

Weathering indices of sedimentary rocks can be used to reconstruct the climate conditions in the source area (Jacobson et al., 2003; Esmaeily et al., 2010; Moosavirad et

Table 3. Trace element concentrations (μg/g) for the aluminous argillites and the underlying limestone samples of the Taiyuan Formation.

Elements	Z-3	Z-4	Z-5	Z-6	Z-7	Z-8	Z-9	Z-10	Z-11	Z-12	Z-13
V	423	329.45	317.25	395.75	425.25	379.5	421.75	470.25	96	114.98	104.23
Cr	117.9	102.3	115.18	125	77.93	94.18	97.38	104.15	24.22	26.4	45.6
Ni	53.08	44.73	17.02	22.47	28.93	34.18	48.88	52.73	40.6	48.05	81.65
Sr	77.95	113.58	12.05	4.85	96.05	75.73	141.3	166.15	4552.5	3727.5	4985
Ba	93.2	92.45	4.03	2.76	111.2	103.93	263.25	310	64.38	58.18	113.88
Zr	244.6	211.38	170.03	225.8	145.1	174.75	171.35	187.95	7.50	8.69	22.86
Nb	6.45	5.12	5.26	5.31	4.09	4.74	5.57	6.18	0.34	0.54	0.66
Hf	7.37	6.69	5.49	7.82	5.25	5.47	5.4	6.22	0.23	0.34	0.78
Ta	4.03	3.38	2.88	2.30	2.62	2.77	3.54	3.87	0.21	2.22	0.49
Th	393.75	412.25	434	174.8	103.55	228.73	219.2	171	7.29	10.18	46.8
La	6.12	5.81	0.43	0.25	0.78	1.48	3.38	2.68	3.7	4.96	1.86
Ce	16.42	14.7	1.93	0.97	1.69	2.41	8.47	6.82	3.53	4.62	1.95
Pr	1.11	1.04	0.14	0.10	0.16	0.28	0.66	0.21	0.73	0.51	0.32
Nd	32.95	31.98	5.29	3.92	5.48	9.53	20.87	16.23	1.50	3.21	1.07
Sm	5.18	5.01	1.31	0.97	0.99	1.61	3.22	2.58	0.43	0.33	0.20
Eu	0.20	0.19	0.04	0.03	0.05	0.07	0.14	0.12	0.15	0.12	0.08
Gd	5.82	5.31	1.09	0.71	0.99	1.81	4.05	3.04	0.3	0.52	0.1
Tb	0.67	0.63	0.15	0.09	0.11	0.18	0.42	0.32	0.08	0.11	0.06
Dy	0.49	0.46	0.13	0.07	0.11	0.27	0.22	1.63	0.39	0.45	0.23
Ho	2.16	2.12	0.58	0.27	0.35	0.45	1.15	0.92	0.10	0.12	0.08
Er	11.45	11.17	2.94	1.29	1.79	2.24	5.79	4.68	0.44	0.27	0.31
Tm	1.15	1.11	0.30	0.13	0.17	0.20	0.54	0.44	0.05	0.04	0.01
Yb	6.21	5.96	1.65	0.68	0.91	0.99	2.73	2.19	0.41	0.24	0.15
Lu	0.90	0.90	0.25	0.09	0.13	0.12	0.38	0.29	0.09	0.02	0.03
V/Cr	3.59	3.22	2.75	3.17	5.46	4.03	4.33	4.52	3.96	4.36	2.29
V/(V+Ni)	0.89	0.88	0.95	0.95	0.94	0.92	0.90	0.90	0.70	0.71	0.56
Sr/Ba	0.84	1.23	2.99	1.75	0.86	0.74	0.54	0.54	70.72	64.07	43.78
La_N/Yb_N	0.09	0.09	0.02	0.03	0.08	0.14	0.12	0.12	0.85	1.95	1.12
Ce/Ce*	1.49	1.42	1.91	1.5	1.15	0.89	1.35	1.38	0.51	0.69	0.60
Eu/Eu*	0.17	0.17	0.17	0.17	0.23	0.19	0.18	0.21	2.01	1.36	2.49

$Ce/Ce^* = Ce_N/(La_N \times Pr_N)^{1/2}$, $Eu/Eu^* = Eu_N/(Pr_N \times Sm_N)^{1/2}$, where N refers to a NASC-normalized value (see Gromet et al., 1984).

al., 2011). Suttner and Dutta (1986) used a binary diagram of SiO_2 vs. (Al_2O_3+K_2O+Na_2O) to reflect the climate conditions in the source area. The studied argillites samples are located in the arid and semiarid field, suggesting that the weathering of source rocks and deposition of argillites occurred in an arid to semiarid climate (Figure 10). According to the paleomagnetic data, the North China Plate, approximately located at a latitude between 15°N and 30°N in the late Carboniferous, was characterized by a subtropical to tropical climate (Liu, 1987).

5.3. Chemical weathering

From the incipient to moderate weathering processes, Ca, Na, and K of the parent rocks are relatively mobile and are easily leached out, resulting in a depletion of these elements and an enrichment of immobile elements. Nesbitt and Young (1982) presented a chemical index of alteration (CIA) to describe the weathering extents of rocks by calculating the mole ratios of alumina to alkaline elements:

$$CIA = [Al_2O_3 / (Al_2O_3 + CaO^* + Na_2O + K_2O)] \times 100,$$

where CaO* represents the CaO content of the silicate phase. The argillite samples have an average value of 91, ranging from 80 to 99, with the highest CIA values in bauxitic argillites. This indicates that the weathering of the parent rocks resulted in more depletion of the labile alkalis and alkali earth elements in bauxitic argillites than aluminous argillites.

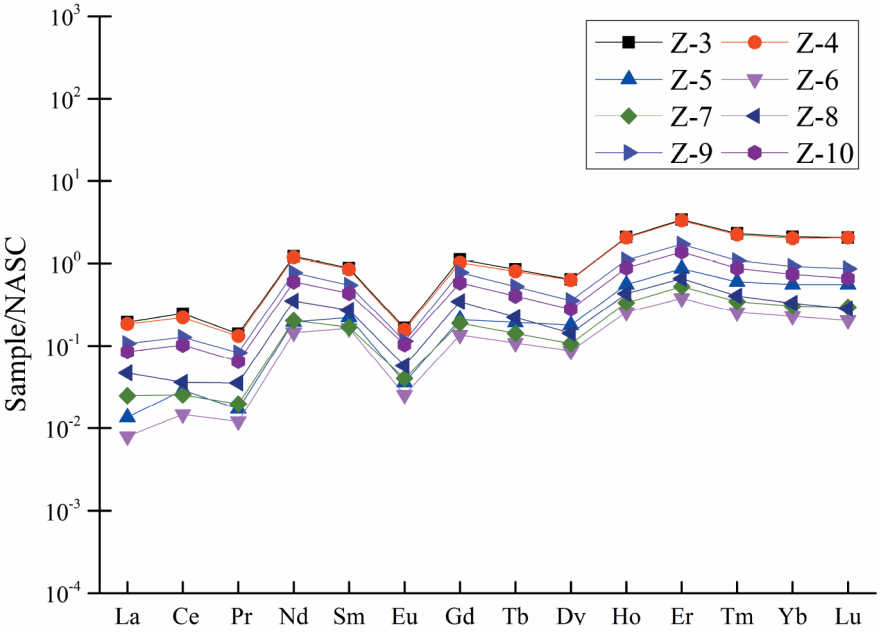

Figure 5. NASC (North American Shale Composite)-normalized REE patterns of the studied aluminous argillite samples. NASC normalizing values are from Gromet et al. (1984).

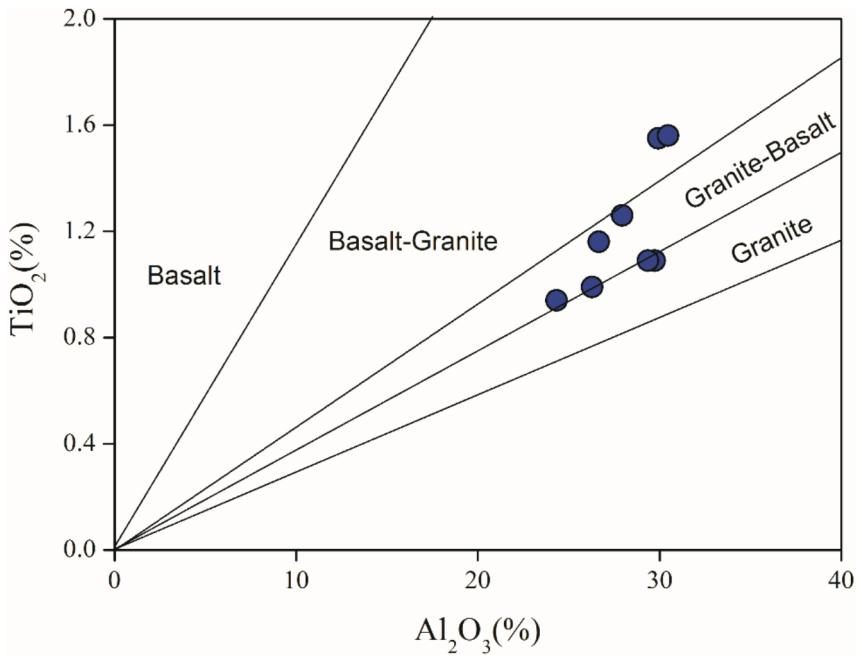

Figure 6. Provenance diagram of Al_2O_3 vs. TiO_2 in the studied aluminous argillites (after Amajor, 1987).

By studying two contrasting basalt profiles, Babechuk et al. (2014) suggested that the A-CN-K triangular diagram can empirically and kinetically predict the chemical weathering direction of rocks. The A-CN-K diagram describes the consequence of chemical weathering of the upper crust where plagioclase and K-feldspar are dissolved, causing depletion of Ca, Na, and K and enrichment of Al (Nesbitt and Young, 1984; Nesbitt, 1992; Babechuk et al., 2014). In Figure 7, the studied argillite samples are located around the Al apex, suggesting an extensive weathering of source rocks. This is consistent with the CIA interpretation.

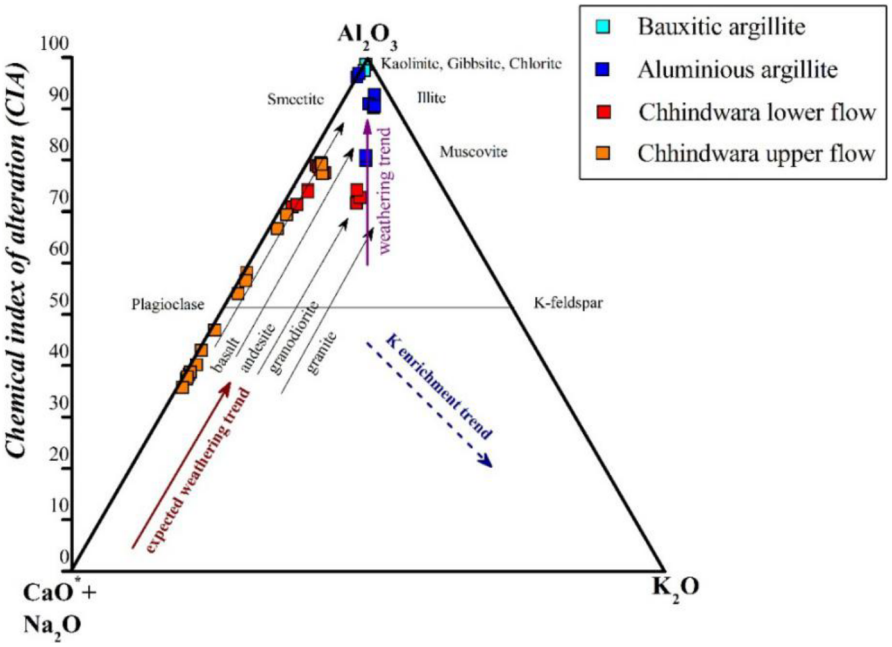

Figure 7. A-CN-K ternary diagram (modified from Nesbitt and Young, 1982; Fedo et al., 1995; Babechuk et al., 2014) showing weathering trends of studies argillites compared to Chhindwara flows (Babechuk et al., 2014).

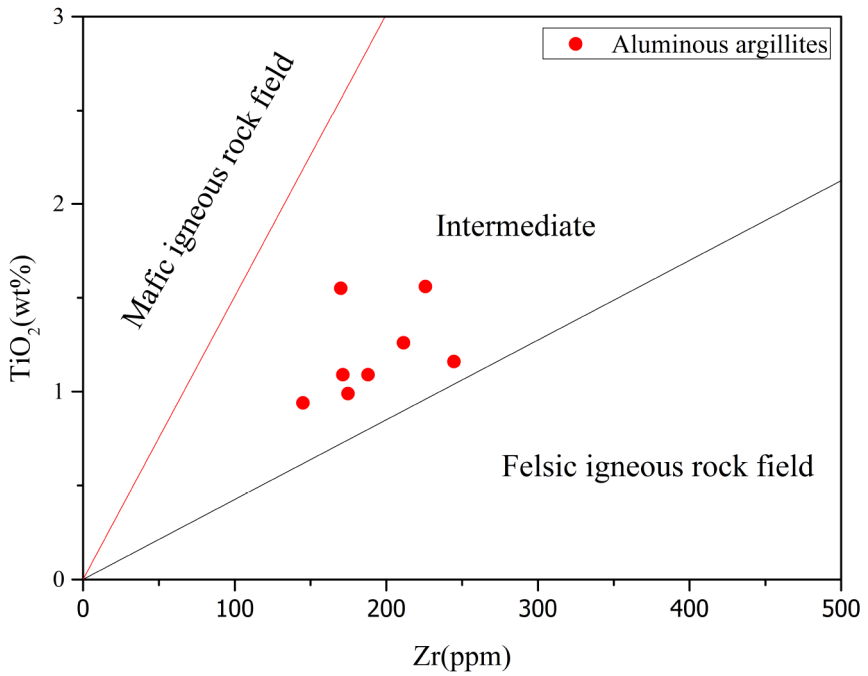

Figure 8. Provenance diagram of TiO_2 vs. Zr in the studied aluminous argillites (after Hayashi et al., 1997).

With the progress of the weathering, Si becomes unstable due to desilication of rocks. The SiO_2-Al_2O_3-TFe_2O_3 (SAF) ternary diagram proposed by Schellmann (1981, 1982, 1986) has been used to quantify the laterization, although there is still debate about the definition and classification of laterization. Based on the SAF ternary diagram, the studied aluminous argillites possibly suffered a weak to moderate laterization (Figure 11).

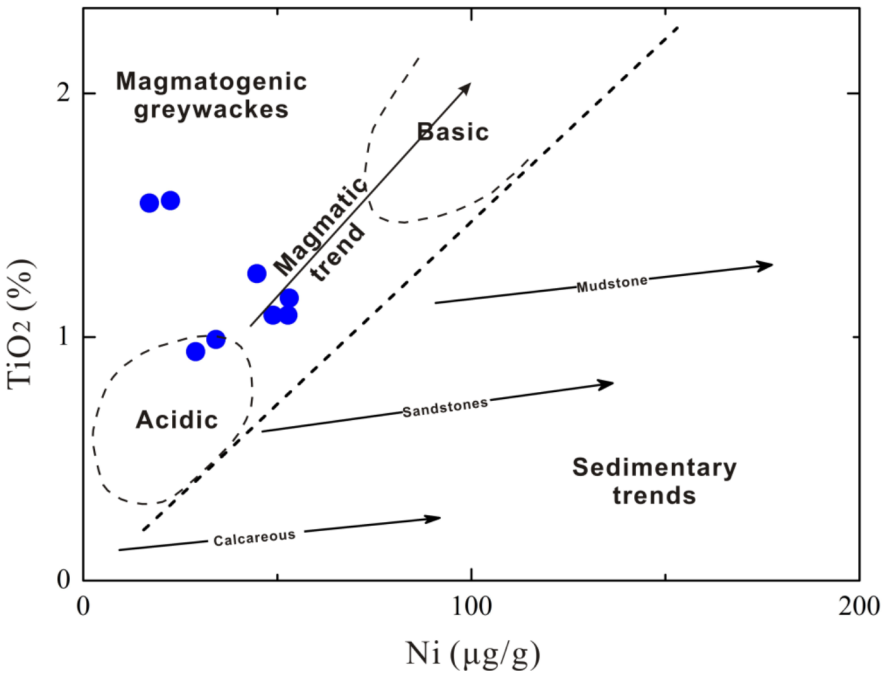

Figure 9. Provenance diagram of TiO_2 vs. Ni in the studied aluminous argillites (after Floyd et al., 1989).

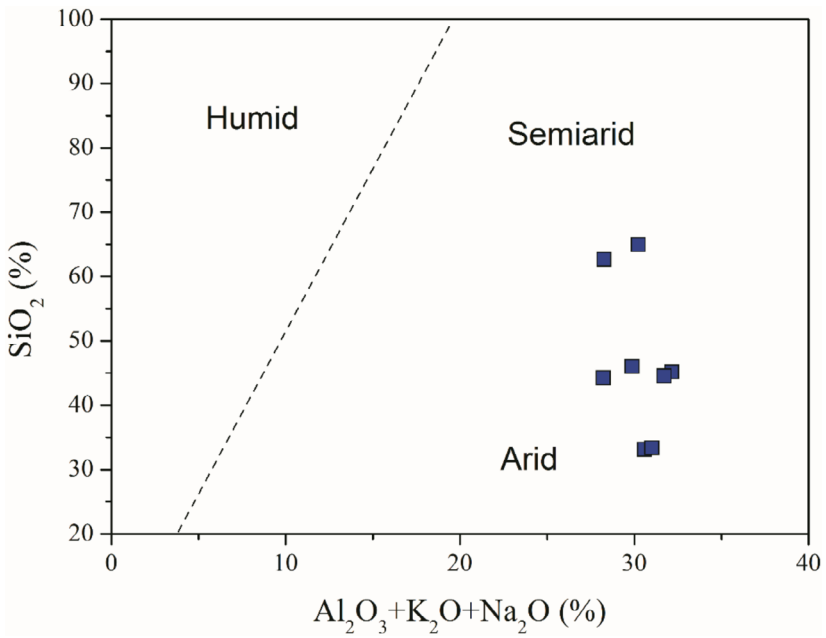

Figure 10. Paleoclimate discrimination diagram of SiO_2 vs. (Al_2O_3+K_2O+Na_2O) in the studied aluminous argillites (after Suttner and Dutta, 1986).

5.4. Depositional environment

Both Sr and Ba are sensitive to variations of paleosalinity, and they are more concentrated in seawater than fresh water (Francois, 1988; Torres et al., 1996; Schmitz et al., 1997). However, the difference in sedimentary environments could separate their correlations. Barium is easily precipitated as $BaSO_4$, while Sr can migrate further because of its higher solubility than that of Ba (Lucas et al., 1990; Van Os et al., 1991). Thus, the Sr/Ba ratio is commonly used to estimate the changes of paleoenvironments of

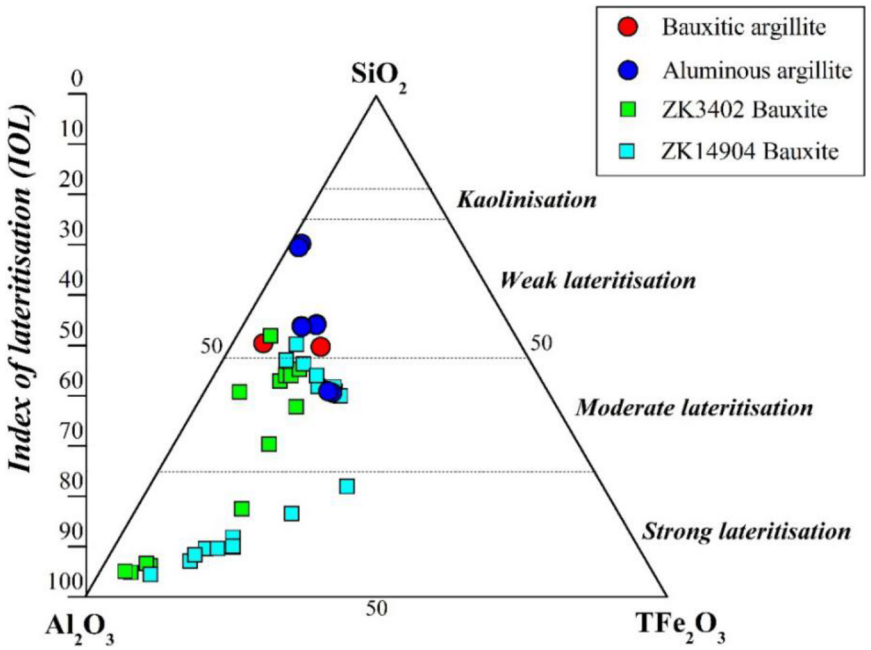

Figure 11. Triangular diagram of SiO_2-Al_2O_3-Fe_2O_3 for the aluminous argillites (modified from Schellmann, 1986 and ZK3402 Bauxite and ZK14904 Bauxite data taken from Wang et al., 2013).

sedimentary rocks (Lan et al., 1988; Raiswell et al., 1988; Van et al., 2003), with Sr/Ba > 1 indicating a marine deposition and Sr/Ba < 1 indicating continental deposition (Van et al., 2003; Jacquet et al., 2005; Paytan et al., 2007; Martinez-Ruiz et al., 2015). The Sr/Ba ratios of the studied argillite samples range from 0.54 to 2.99, with an average value of 1.19, suggesting that they were possibly deposited in an unstable paleodepositional environment that alternated between marine and continental depositional settings (Van et al., 2003; Jacquet et al., 2005; Paytan et al., 2007; Martinez-Ruiz et al., 2015).

The trace elements in the sediment rocks could also be used to infer the depositional environment (Mongenot et al., 1996). Vanadium is usually preserved in porphyrins of organic matter and concentrated in the reducing depositional environments (Calvert and Pedersen, 1993; Jones and Manning, 1994; Tribovillard et al., 2006). Jones and Manning (1994) suggested that the enrichment pattern of Cr is always related to the clastic depositional fraction. Cr mainly exists as Cr^{6+} in oxic environments and as Cr^{3+} in anoxic conditions. Jones and Manning (1994) proposed to use V/Cr ratios to estimate the paleoredox depositional conditions, with V/Cr < 2 indicating an oxidizing condition, 2 < V/Cr < 4.25 indicating a poor oxygen sedimentary environment, and V/Cr > 4.25 indicating a reducing environment. The V/Cr ratios of the studied aluminous argillites range from 2.75 to 5.46 with an average value of 3.88, suggesting that the studied aluminous argillites were deposited in a suboxic to anoxic depositional environment. The paleoredox depositional environment can also be identified by the V/(V+Ni) ratio (Dill et al., 1988; Hatch and Leventhal, 1992; Jones et al., 1994). The V/(V+Ni) ratio of 0.46 is considered as the transition boundary from oxic to suboxic and anoxic depositional environments. The V/(V+Ni) ratios of the studied argillites range from 0.88 to 0.95, with an average value of 0.92, suggesting an anoxic environment. Similarly, the redox-sensitive element Ce can also be used to indicate the redox environments (Wilde et al., 1996; Yang et al., 1999; Feng et al., 2000). In an oxidizing environment, Ce^{3+} can be oxidized to Ce^{4+} and then preserved by the precipitation of cerianite (CeO_2). In contrast, other trivalent REEs are commonly leached out due to their relatively high solubility (Braun et al., 1990). The positive Ce anomalies in our studied aluminous argillites suggest that they were deposited in an oxic environment. However, this contradicts the suboxic to anoxic environments as inferred from V/Cr and V/(V+Ni). We speculate that these argillites were initially weathered under anoxic conditions. The subsequent suboxic to anoxic condition redistributed the relationship between trace elements rather than REEs. One of the aluminous argillites (Z-8) shows a slightly negative Ce anomaly of 0.89, which was probably caused by postdepositional processes such as the leaching of argillites by groundwater or hydrothermal fluids.

6. Conclusions

In this study, we investigated the elemental geochemistry of argillites layers from the Late Carboniferous Taiyuan Formation, Huainan Coalfield, and the following conclusions were obtained:

1) The studied argillites are mainly composed of Al_2O_3 and SiO_2. The La_N/Yb_N values of all the aluminous argillites are less than 0.4, exhibiting a significant enrichment of HREEs relative to LREEs. All aluminous argillites show positive Ce anomalies ($Ce/Ce^* = 1.39$) and negative Eu anomalies ($Eu/Eu^* = 0.19$, ranging from 0.17 to 0.23).

2) The oxides and trace elements suggest that the studied aluminous argillites from different layers derived from the same sedimentary sources. The TiO_2 vs. Ni, Al_2O_3 vs. TiO_2, and A-CN-K triangular diagrams indicate that these aluminous argillites were probably sourced from felsic to intermediate igneous rocks.

3) The binary diagram of SiO_2 vs. (Al_2O_3+K_2O+Na_2O) indicates that the studied argillites were probably formed under an arid to semiarid climate. The CIA values and the A-CN-K diagrams suggest that these argillites were formed by extremely chemical weathering products.

4) A series of geochemical indices including the Sr/Ba, V/Cr, and V/(V+Ni) ratios and the Ce anomalies show that the aluminous argillites were deposited in a suboxic to anoxic environment.

Acknowledgments

The authors acknowledge the support from the National Basic Research Program of China (973 Program, 2014CB238903) and the National Natural Science Foundation of China (No. 41173032 and No. 41373110) and the Anhui Provincial Natural Science Foundation (1408085MD69). We acknowledge the editors and reviewers for polishing the language of the paper and for in-depth discussions.

References

Abedini A, Calagari AA (2014). REE geochemical characteristics of titanium-rich bauxites: the Permian Kanigorgeh horizon, NW Iran. Turkish J Earth Sci 23: 513-532.

Amajor LC (1987). Major and trace elements geochemistry of Albin and Turonian shales from the Southern Benue trough, Nigeria. J Afr Earth Sci 6: 633-641.

Armstrong-Altrin JS, Lee YI, Verma SP, Ramasamy S (2004). Geochemistry of sandstones from the upper Miocene Kudankulam Formation, southern India: Implications for provenance, weathering, and tectonic setting. J Sediment Res 74: 285-297.

Babechuk MG, Widdowson M, Kamber BS (2014). Quantifying chemical weathering intensity and trace element release from two contrasting basalt profiles, Deccan Traps, India. Chem Geol 263: 56-75.

Braun JJ, Pagel M, Muller JP, Bilong P, Michard A, Guillet B (1990). Cerium anomalies in lateritic profiles. Geochim Cosmochim Acta 54: 781-795.

Calagari AA, Abedini A (2007). Geochemical investigations on Permo-Triassic bauxite horizon at Kanisheeteh, east of Bukan, West-Azarbaidjan, Iran. J Geochem Explor 94: 1-18.

Calvert SE, Pedersen TF (1993). Geochemistry of recent oxic and anoxic marine sediments: implications for the geological record. Mar Geol 113: 67-88.

Chen J, Liu G, Jiang M, Chou CL, Li H, Wu B, Zheng LG, Jiang D (2011). Geochemistry of environmentally sensitive trace elements in Permian coals from the Huainan coalfield, Anhui, China. Int J Coal Geol 88: 41-54.

Dhannoun HY, Al-Dlemi AM (2013). The relation between Li, V, P_2O_5, and Al_2O_3 contents in marls and mudstones as indicators of environment of deposition. Arab J Geo Sci 6: 817-823.

Dill H, Teschner M, Wehner H (1988). Petrography, inorganic and organic geochemistry of Lower Permian carbonaceous fan sequences ("Brandschiefer Series") Federal Republic of Germany: constraints to their paleogeography and assessment of their source rock potential. Chem Geol 67: 307-325.

Dobrzinski N, Bahlburg H, Strauss H, Zhang, Q (2004). Geochemical climate proxies applied to the Neoproterozoic glacial succession on the Yangtze Plateform, South China. In: Jenkins GL, McMenamin MAS, McKay CP, Sohl L, editors. The Extreme Proterozoic: Geology, Geochemistry, and Climate. AGU Monograph. New York, NY, USA: Wiley, pp. 13-32.

El-Bialy MZ (2013). Geochemistry of the Neoproterozoic metasediments of Malhaq and Um Zariq formations, Kid metamorphic complex, Sinai, Egypt: implications for source-area weathering, provenance, recycling, and depositional tectonic setting. Lithos 175: 68-85.

Esmaeily D, Rahimpour-Bonab H, Esna-Ashari A, Kananian A (2010). Petrography and geochemistry of the Jajarm Karst Bauxite Ore Deposit, NE Iran: implications for source rock material and ore genesis. Turkish J Earth Sci 19: 267-284.

Fedo CM, Nesbitt HM, Young GM (1995). Unraveling the effects of potassium metasomatism in sedimentary rocks and paleosols, with implications for paleoweathering conditions and provenance. Geology 23: 921-924.

Feng H, Erdtmann BD, Wang H (2000). Early Paleozoic whole-rock Ce anomalies and secular eustatic changes in the Upper Yangtze region. Science in China Series D 43: 328-336.

Floyd PA, Leveridge BE (1987). Tectonic environment of the Devonian Gramscatho basin, south Cornwall: framework mode and geochemical evidence from turbiditic sandstones. J Geol Soc London 144: 531-542.

Floyd PA, Shail R, Leveridge BE, Franke W (1991). Geochemistry and provenance of Rhenohercynian synorogenic sandstones: implications for tectonic environment discrimination. In: Morton AC, Todd SP, Haughton PDW, editors. Developments in Sedimentary Provenance Studies. London, UK: Geological Society Special Publication 57, pp. 173-188.

Floyd PA, Winchester JA, Park RG (1989). Geochemistry and tectonic setting of Lewisian clastic metasediments from the early Proterozoic Loch Maree Group of Gairloch, NW Scotland. Precambrian Res 45: 203-214.

Francois R (1988). A study on the regulation of the concentrations of some trace metals (Rb, Sr, Zn, Pb, Cu, V, Cr, Ni, Mn and Mo) in Saanich Inlet sediments, British Columbia, Canada. Mar Geol 83: 285-308.

Ghabrial DS, Samuel MD, Moussa HE (2012). Geochemistry and tectonic setting of early Pan-African metamorphosed volcano-sedimentary sequence in southern Solaf zone, SW Sinai, Egypt. Arab J Geo Sci 6: 3635-3649.

Gromet LP, Dymek RF, Haskin LA, Korotev RI (1984). The 'North American Shale Composite': its compilation, major and trace element characteristics. Geochim Cosmochim Acta 48: 2469-2482.

Harnois L (1988). The CIW index: a new chemical index of weathering. Sediment Geol 55: 319-322.

Hatch JR, Leventhal JS (1992). Relationship between inferred redox potential of the depositional environment and geochemistry of the Upper Pennsylvanian (Missourian) Stark Shale Member of the Dennis Limestone, Wabaunsee County, Kansas, USA. Chem Geol 99: 65-82.

Hayashi KI, Fujisawa H, Holland HD, Ohmoto H (1997). Geochemistry of ~1.9 Ga sedimentary rocks from northeastern Labrador, Canada. Geochim Cosmochim Acta 61: 4115-4137.

Imchen W, Thong GT, Pongen T (2014). Provenance, tectonic setting and age of the sediments of the Upper Disang Formation in the Phek District, Nagaland. J Asian Earth Sci 88: 11-27.

Jacobson AD, Blum JD, Chamberlain CP, Craw D, Koons PO (2003). Climatic and tectonic controls on chemical weathering in the New Zealand Southern Alps. Geochim Cosmochim Acta 67: 29-46.

Jacquet SHM, Dehairs F, Cardinal D, Navez J, Delille B (2005). Barium distribution across the Southern Ocean frontal system in the Crozet-Kerguelen Basin. Mar Chem 95: 149-162.

Jolly WT (1980). Development and degradation of Archean lavas, Abitibi area, Canada, in light of major element geochemistry. J Petrol 21: 323-363.

Jones B, Manning DA (1994). Comparison of geochemical indices used for the interpretation of palaeoredox conditions in ancient mudstones. Chem Geol 111: 111-129.

Lafleche MR, Dupuy C, Bougault H (1992). Geochemistry and petrogenesis of Archean mafic volcanic rocks of the southern Abitibi belt, Quebec. Precambrian Res 57: 207-241.

Lan C, Yang B, Peng S (1988). Environment for forming major coal-seams of Permian coal-bearing series in Huainan coalfield. J China Coal Soc 1: 11-22 (in Chinese with an English abstract).

Liu C (1987). Genetic type of Chinese bauxite. Sci China (Series B) 5: 535-544 (in Chinese).

Lucas J, El Faleh EM, Prévôt L (1990). Experimental study of the substitution of Ca by Sr and Ba in synthetic apatites. In: Notholt AJG, editor. Phosphorite Research and Development. London, UK: Geological Society Special Publication 52, pp. 33-47.

Martinez-Ruiz F, Kastner M, Gallego-Torres D, Rodrigo-Gámiz M, Nieto-Moreno V, Ortega-Huertas M (2015). Paleoclimate and paleoceangraphy over the past 20,000 yr in the Mediterranean Sea Basins as indicated by sediment elemental proxies. Quaternary Sci Rev 107: 25-46.

McLennan SM (1993).Weathering and global denudation. J Geol 101: 295-303.

Meinhold G, Howard JP, Strogen D, Kaye MD, Abutarruma Y, Elgadry M, Thusu B, Whitham AG (2013). Hydrocarbon source rock potential and elemental composition of lower Silurian subsurface shales of the eastern Murzuq Basin, southern Libya. Mar Petrol Geol 48: 224-246.

Mongenot T, Tribovillard NP, Desprairies A, Lallier-Vergès E, Laggoun-Defarge F (1996). Trace elements as palaeoenvironmental markers in strongly mature hydrocarbon source rocks: the Cretaceous La Luna Formation of Venezuela. Sediment Geol 103: 23-37.

Moosavirad SM, Janardhana MR, Sethumadhav MS, Moghadam MR, Shankara M (2011). Geochemistry of lower Jurassic shales of the Shemshak Formation, Kerman Province, Central Iran: provenance, source weathering and tectonic setting. Chem Erde-Geochem 71: 279-288.

Nath BN, Bau M, Rao BR, Rao CM (1997). Trace and rare earth elemental variation in Arabian Sea sediments through a transect across the oxygen minimum zone. Geochim Cosmochim Acta 61: 2375-2388.

Nath BN, Kunzendorf H, Pluger WL (2000). Influence of provenance, weathering, and sedimentary processes on the elemental ratios of the fine-grained fraction of the bedload sediments from the Vembanad Lake and the adjoining continental shelf, southwest coast of India. J Sediment Res 70: 1081-1094.

Nesbitt HW (1992). Diagenesis and metasomatism of weathering profiles, with emphasis on Precambrian paleosols. In: Martin IP, Chesworth W, editors. Weathering, Soils & Paleosols. Amsterdam, the Netherlands: Elsevier, pp. 127-152.

Nesbitt HW, Young GM (1982). Early Proterozoic climates and plate motions inferred from major element chemistry of lutites. Nature 299: 715-717.

Nesbitt HW, Young GM (1984). Prediction of some weathering trends of plutonic and volcanic rocks based on thermodynamic and kinetic considerations. Geochim Cosmochim Acta 48: 1523-1534.

Nesbitt HW, Young GM (1989). Formation and diagenesis of weathering profiles. J Geol 97: 129-147.

Panahi A, Young GM, Rainbird RH (2000). Behavior of major and trace elements (including REE) during Paleoproterozoic pedogenesis and diagenetic alteration of an Archean granite near Ville Marie, Quebec, Canada. Geochim Cosmochim Acta 64: 2199-2220.

Paradis S, Ludden J, Gelinas L (1988). Evidence for contrasting compositional spectra in comagmatic intrusive and extrusive rocks of the late Archean Blake River Group, Abitibi, Quebec. Canadian J Earth Sci 25: 134-144.

Paytan A, Averyt K, Faul K, Gray E, Thomas E (2007). Barite accumulation, ocean productivity, and Sr/Ba in barite across the Paleocene-Eocene Thermal Maximum. Geology 35: 1139-1142.

Raiswell R, Buckley F, Berner RA, Anderson TF (1988). Degree of pyritisation of iron as a paleoenvironmental indicator of bottom-water oxygenation. J Sediment Res 58: 812-819.

Schellmann W (1981). Considerations on the definition and classification of laterites. A critique of the Schellmann definition and classification of laterite. Catena 47: 117-131.

Schellmann W (1982). Eine neue Lateritdefinition. Geol Jahrb D 58: 31-47 (in German).

Schellmann W (1986). A new definition of laterite. Geol Surv India Mem 120: 1-7.

Schmitz B, Charisi SD, Thompson EI, Speijer RP (1997). Barium, SiO_2 (excess), and P_2O_5 as proxies of biological productivity in the Middle East during the Palaeocene and the latest Palaeocene benthic extinction event. Terra Nova 9: 95-99.

Stone WE, Jensen LS, Church WR (1987). Petrography and geochemistry of an unusual Fe-rich basaltic komatiite from Boston Township, northeastern Ontario. Canadian J Earth Sci 24: 2537-2550.

Sun R, Liu G, Zheng L, Chou CL (2010). Geochemistry of trace elements in coals from the Zhuji Mine, Huainan Coalfield, Anhui, China. Int J Coal Geol 81: 81-96.

Suttner LJ, Dutta PK (1986). Alluvial sandstone composition and paleoclimate, I. Framework mineralogy. J Sediment Res 56: 329-345.

Taylor SR, McLennan SM (1995). The geochemical evolution of the continental crust. Rev Geophys 33: 241-265.

Torres ME, Brumsack HJ, Bohrman G, Emeis KC (1996). Barite fronts in continental margin sediments: a new look at barium remobilization in the zone of sulfate reduction and formation of heavy barites in diagenetic fronts. Chem Geol 127: 125-139.

Tribovillard N, Algeo TJ, Lyons T, Riboulleau A (2006). Trace metals as paleoredox and paleoproductivity proxies: an update. Chem Geol 232: 12-32.

Van BP, Reyss JL, Bonte P, Schmidt S (2003). Sr/Ba in barite: a proxy of barite preservation in marine sediments?. Mar Geol 199: 205-220.

van Os BJ, Middelburg JJ, de Lange GJ (1991). Possible diagenetic mobilization of barium in sapropelic sediments from the eastern Mediterranean. Mar Geol 100: 125-136.

Wang X, Jiao Y, Du Y, Ling W, Wu L, Cui T, Zhou Q, Jin Z, Lei Z, Weng S (2013). REE mobility and Ce anomaly in bauxite deposit of WZD area, Northern Guizhou, China. J Geochem Explor 133: 103-117.

Wilde P, Quinby-Hunt MS, Erdtmann BD (1996). The whole-rock cerium anomaly: a potential indicator of eustatic sea-level changes in shales of the anoxic facies. Sediment Geol 101: 43-53.

Yang J, Sun W, Xue Y, Tao X (1999). Variations in Sr and C isotopes and Ce anomalies in successions from China: evidence for the oxygenation of Neoproterozoic seawater?.Percambrian Res 93: 215-233.

Yang M, Liu G, Sun R, Chou CL, Zheng L (2011). Characterization of intrusive rocks and REE geochemistry of coals from the Zhuji Coal Mine, Huainan Coalfield, Anhui, China. Int J Coal Geol 94: 283-295.

Young GM (2013). Secular changes at the Earth's surface; evidence from palaeosols, some sedimentary rocks, and palaeoclimatic perturbations of the Proterozoic Eon. Gondwana Res 24: 453-467.

Zimmermann U, Bahlburg H (2003). Provenance analysis and tectonic setting of the Ordovician clastic deposits in the southern Puna Basin, NW Argentina. Sedimentology 50: 1079-1104.